Parameterisation and transformation of wave asymmetries over a low-crested breakwater

Parameterisation and transformation of wave asymmetries over a low-crested breakwater

Zhong Peng, Qingping Zou *, Dominic Reeve, Baoxing Wang

C-CoDE, School of Engineering, University of Plymouth, Plymouth, UK

A B S T R A C T

This paper presents the results of an investigation of the transformation of wave skewness and asymmetry as waves propagate obliquely over low-crested breakwaters, (LCBs), based on an analysis of measurements collected in the DELOS project. Considering the effect of the local Ursell number on wave asymmetries, a set of practical empirical formulae were established using least squares regression for both smooth and rubble mound LCBs. Predictions are in good agreement with measurements. Wave skewness on both sides of LCBs is linearly correlated for rubble mound LCBs but weakly correlated for smooth LCBs. While wave asymmetry on both sides of LCBs has a weakly quadratic correlation. The effect of the relative freeboard on the relationships of wave asymmetries between both sides is significant for rubble mound LCBs, but the same does not hold for smooth LCBs. With the presence of LCBs, wave skewness retains a positive sign on both sides but asymmetry changes from negative on the incident side to positive on the transmission side. Bispectral analysis shows that positive skewness and negative asymmetry arises from self–self and sum interactions but positive asymmetry is due to difference interactions between frequencies. The findings provide improved understanding of changes in wave skewness and asymmetry in the vicinity of structures, which may help mitigate scour and improve the stability of breakwaters.

1. Introduction

One objective of the European project DELOS (Environmental Design of Low Crested Coastal Defence Structures, EVK3-CT-2000-00041, http://www.delos.unibo.it) was to promote effective design of low-crested breakwaters, (LCBs), as a method of shoreline defence which also preserved the littoral environment and coast economic development. A better understanding of wave transformation over low-crested breakwaters is crucial in the assessment of the functionality and stability of coastal and flood defence schemes. Previous studies, however, have mainly been on wave transmission, reflection and wave spectral change over LCBs (Van der Meer et al., 2000, 2005; Wang et al., 2007). Literature on the transformation of wave skewness and asymmetry over LCBs is sparse.

Cornish (1898) observed that the onshore velocity under wave crests was more effective at moving coarse sediment than the seaward velocity related to wave troughs. This observation was consistent with the theory of Stokes (1847): the onshore velocity related to a wave crest is larger and of shorter duration than the seaward velocity associated with a wave trough, arising from a wave shape characterised by peaked crests and flat troughs. The lack of symmetry of a wave profile relative to the horizontal axis is called wave skewness. On the other hand, waves with a steep front face and gentle rear face were described as pitch forward waves and vice versa. The lack of symmetry of a wave profile relative to the vertical axis is called wave asymmetry. Elgar and Guza (1985) proposed that wave asymmetry can be calculated from the skewness of the Hilbert transform of wave time series.

It has long been recognised that wave skewness and asymmetry are directly related to sediment transport and subsequent changes in beach morphology. Understanding and modelling the near shore wave shape characteristics around LCBs are central to the application and development of physically-based models of sediment transport that aim to simulate the evolution of cross-shore beach profiles. Inman and Bagnold (1963) were the first to apply the concept of a skewed velocity field to the modelling of beach equilibrium; Bagnold (1966) later applied this concept to predict the total bedload transport. Wilson (1966) showed that the net bedload transport rate is proportional to the third moment of near-bed free-stream velocity. Subsequently, higher moments of the velocity field were incorporated into models of total bedload transport by Bowen (1980) and Bailard and Inman (1981). Nielsen (1992) noted that the onshore velocity of a pitch forward wave increases in magnitude faster than the offshore velocity, and the associated boundary layer has a shorter time to develop. Thus, the onshore velocity generates a thinner boundary layer and therefore a larger sediment transport. Drake and Calantoni (2001) found that differences in acceleration between the front and the back of an asymmetric wave yield horizontal pressure gradients in the boundary layer, which act on the near-bed fluid and sediment. This led Nielsen and Callaghan (2003) to conclude that the

* Corresponding author. Tel.: +44 1752 586158; fax: +44 1752 586101.
E-mail address: qingping.zou@plymouth.ac.uk (Q. Zou).

acceleration effects, associated with the saw-tooth asymmetry of the flume waves, account for the greatest part of the sediment transport.

Christou et al. (2008) concluded that highly nonlinear processes are involved in the evolution of waves propagating over a breakwater. The bispectrum can determine wave skewness and asymmetry arising from wave–wave nonlinear interactions. Bispectral analysis of previous studies showed that nonlinear interactions including self interactions, sum and difference interactions determined the sign and amplitude of wave skewness and asymmetry (Elgar and Guza, 1985; Crawford, 2000; Crawford and Hay, 2001). Based on the bispectral analysis of data sets for natural beach, Doering and Bowen (1995) derived empirical relationships of wave skewness and asymmetry with the Ursell number. Herbers et al. (2003) used a Boussinesq model to investigate the nonlinear transformation of the frequency-directional spectrum and bispectrum of surface gravity waves propagating over a submerged sand bar on a beach. Their Boussinesq model predicted surf zone skewness and asymmetry well. Zou et al. (2003) derived the analytical solutions of wave orbital velocity for the entire water column over a sloping bottom. Both their theory and observations showed that the skewness and asymmetry of the vertical velocity are subject to significant bottom slope effects, whereas those of horizontal velocity are not. However, these studies focused on wave skewness and asymmetry on natural beaches; the effect of coastal structures on wave skewness and asymmetry has not been investigated.

Therefore, the aim of this present work is to investigate the transformation of wave asymmetries over smooth and rubble mound LCBs. A set of empirical formulae of wave asymmetries will be derived for practical use using laboratory data sets collected in the DELOS project. Bispectral analysis will be introduced to investigate the contribution of nonlinear interactions between frequency components of wave spectrum to wave skewness and asymmetry.

2. Experiment

Data was obtained from oblique three-dimensional wave transmission tests in the multidirectional wave basin (18.0 m × 12.0 m × 1.0 m) at Aalborg University, Denmark. Detailed descriptions about this project can be found in Wang (2003), Kramer et al. (2005) and the DELOS website (http://www.delos.unibo.it/).

A smooth mound low-crested breakwater, and a rubble low-crested breakwater, were tested. The cross-section and layouts of smooth and rubble mound LCBs including positions of gauges are given in Kramer et al. (2005). Fig. 1 shows the cross-section and layouts of a smooth LCB. The target irregular 3-D waves were generated using the parameterised Jonswap spectrum and spreading function of cosine distribution with spreading parameter $s = 50$. Layouts of breakwaters with 0°, 30° and 50° relative to the wave generator were used to cover a large range of wave incident angles. Table 1 lists an overall view of 74 tests of short-crested and 10 tests of long-crested irregular waves. Each record was sampled at 40 Hz and was 90-second long. The observations were measured from ten fixed gauges, five of them located on the incident side of LCBs and the other five gauges located on the transmission side of LCBs (Fig. 1). A bandpass filtering (the upper and lower cut-off frequencies are 5 and 0.2 times the peak frequency respectively) was applied to the measurements to remove the noise and signal which are separated in the temporal frequency domain.

Table 1
Overall view of test program.

Parameters	Values
No. of tests	168
Crest freeboard (m)	0.05, 0, −0.05
Water depth (m) (rubble mound LCBs)	0.20,0.25,0.30
Water depth (m) (smooth LCBs)	0.25,0.30,0.35
Wave height (m)	0.06 to 0.22
Wave steepness	0.02 to 0.058
Wave peak period (s)	1.06 to 2.33
Wave mean period (s)	0.9 to 1.8
Incidence angles (°)	0 to 60

3. Transformation of wave skewness and asymmetry over LCBs

Wave skewness and asymmetry describe the lack of symmetry of a wave profile relative to the horizontal and vertical axes respectively. The skewness can be obtained from the third moment of surface elevation normalized by the second moment of surface elevation to the power of 1.5. Wave asymmetry can be calculated as the skewness of Hilbert transform of surface elevation (Elgar and Guza, 1985). As shown in Fig. 2, waves are characterised by a gradual peaking of crests and flattening of troughs at both sides of breakwaters, a characteristic of positive wave skewness (Elgar and Guza, 1985). Also, waves pitch forward on the incident side, but pitch backward on the transmission side, a characteristic of negative and positive asymmetries respectively.

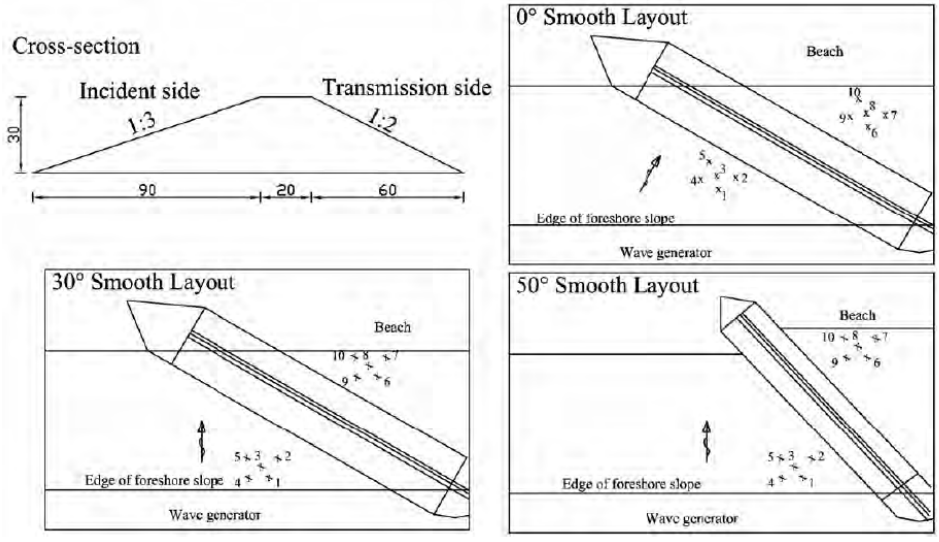

Fig. 1. Cross-section and layouts of smooth LCBs including positions of gauges, 'x' marks the position of wave gauges (Kramer et al., 2005).

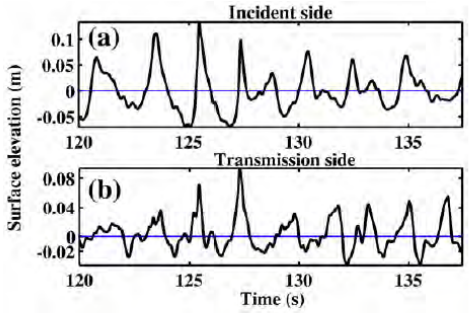

Fig. 2. Surface elevations measured in (a) gauge 2 on the incident side and (b) gauge 7 on the transmission side of smooth LCBs. Freeboard is 0 m, incident wave height is 0.14 m, water depth is 0.3 m and incident angle is 0°.

The transmitted wave train has greater high frequency content than the incident wave train, as observed by Van der Meer et al. (2005).

Parameters involved in wave transmission over LCBs, such as incident wave height (preferably the value of H_s at the location of gauge 1), incident wave angles (α), Iribarren number ($\xi = \tan(\beta)/(sop)^{0.5}$, where β is the seaside slope of structures and sop is the wave steepness in deep water), structural freeboards (R_c), crest width (B) and nominal diameters of rubbles (D_{n50}), were found to be important in wave transmission process (Van der Meer et al., 2005). A definition sketch is given in Fig. 3.

However, parameters mentioned above are global and their effects on wave–structure interaction are reflected in the local wave parameters. For instance, the effect of incident wave angles is mainly on the transmission coefficient, and consequently the transmitted wave heights, which is consistent with the conclusions of Van der Meer et al. (2005). In addition, based on the bispectral analysis, Elgar and Guza (1985) concluded that wave asymmetries were due to self–self interactions, sum frequency interactions and different frequency interactions. Therefore, wave asymmetries are a measure of wave nonlinearity. The nonlinear interaction between two primary wave-trains can induce a second-order Stokes wavetrain (Phillips, 1960), and the Ursell number (the relative wave height times the relative wavelength squared) is the expansion parameter for a Stokes wavetrain. Thus the Ursell number indicates the wave nonlinearity. As a result, we will next look at the relationship between wave skewness or asymmetry and local Ursell number, which has been applied to parameterize orbital velocity asymmetries of shoaling and breaking waves on natural beaches in Doering and Bowen (1995) and Doering et al. (2000). Although it has been observed that gentler beach leads to more symmetric wave profile, this study does not consider the slope effect of LCBs, since in the DELOS experiments the smooth LCB has only one seaside slope of 1:3, and the rubble mound LCB has only one seaside slope of 1:2 as well.

Van der Meer et al. (2005) pointed out that more energy is distributed around higher frequencies than in the incident spectrum due to the effect of wave breaking over a low-crested breakwater. As a result, although the wave peak period on the transmission side (the reverse of peak frequency of wave spectrum) is close to the wave peak period on the incident side, the mean period ($T_{m01} = 2*\pi*m_0/m_1$, where m_0 is the zero order moment and m_1 is the first order moment of power spectrum) may decrease considerably. Therefore, a local Ursell number calculated with peak period does not contain the information of wave period changes over the LCBs. Wave mean period is used to calculate the local Ursell number instead. Thus, the definition of local Ursell number, U_r, in the present work is:

$$U_r = \frac{H_s L_m^2}{h^3} \tag{1}$$

where H_s is defined here as the average height of the highest one-third of the waves in 900s for each gauge, L_m is the local mean wavelength calculated by the mean period and h is the local water depth.

It can be expected that wave skewness on the incident side (S_i) and asymmetry on the incident side (A_i) of LCBs will show a similar relationship with respect to the Ursell number on the incident side (U_{ri}) as that of wave shoaling on a natural beach. Doering and Bowen (1995) obtained the relationship between wave asymmetries and the Ursell number, and argued that the asymmetries at each depth are under strong local control. Fig. 4 shows that the comparisons between Eqs. (4.10) and (4.11) in Doering and Bowen (1995) and DELOS data on the incident side of both smooth and rubble mound LCBs. Note that the Ursell number in Doering and Bowen (1995) was calculated by peak period and also different from the present definition (Eq. (1)) by a factor $3/(32\pi)$. Fig. 4 shows that the equations derived by Doering and Bowen (1995) underestimate wave skewness and absolute asymmetry. It is worth mentioning that Eqs. (4.10) and (4.11) in Doering and Bowen (1995) are empirical formulae derived from field measurements of a natural beach in the absence of low-crested breakwaters.

3.1. Transformation of wave skewness and asymmetry over smooth LCBs

Fig. 5a shows that wave skewness is positive and increases rapidly with increasing Ursell number, attains a maximum and then stays around the maximum. While wave asymmetry fluctuates around zero at small Ursell number, then becomes negative and decays with increasing the Ursell number (Fig. 5c). These results are similar to those of the natural beach (Doering and Bowen, 1995; Doering et al., 2000). Because of its similarity to saturation characteristics, the relationship between wave skewness and asymmetry and the Ursell number is followed by a hyperbolic tangent law. Using the DELOS data, Eq. (2) ($R^2 = 0.69$) and Eq. (3) ($R^2 = 0.84$) are established from measurements on the incident side with least squares fitting and provide quantitative relationships between S_i and A_i with respect to U_{ri}. The range of Ursell number on the incident side is between 5 and 43.

$$S_i = 1.28*\tanh\left(\frac{-3.17}{U_{ri}}\right) + 0.10 \tag{2}$$

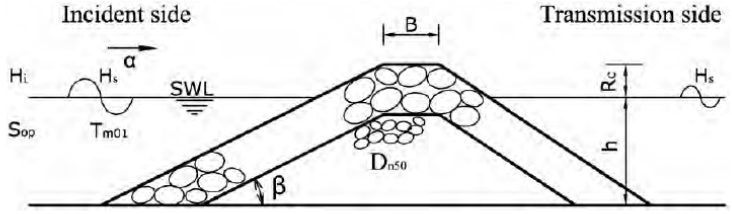

Fig. 3. Definitions of governing parameters involved in wave transmission over LCBs (Van der Meer et al., 2005).

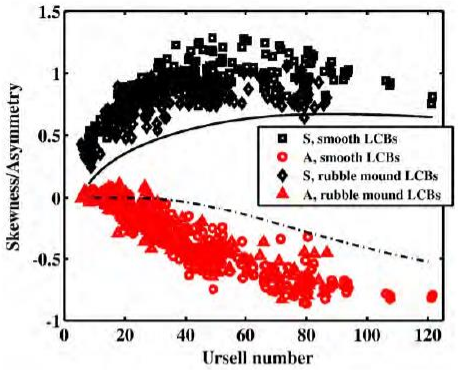

Fig. 4. Comparison between Eqs. (4.10) (solid line) and (4.11) (dash-dotted line) in Doering and Bowen (1995) and DELOS data on the incident side of both smooth and rubble mound LCBs. Note, the definition of Ursell number here is calculated by the peak period in order to keep the same as that in Doering and Bowen (1995).

$$A_i = -1.53^{*}\tanh\left(\frac{-22.87}{U_{ri}}\right) - 1.52. \tag{3}$$

It is expected that the relationship between wave skewness on the transmission side (S_t) and wave asymmetry on the transmission side (A_t) and the local Ursell number on the transmission side (U_{rt}) is not similar to that on the incident side due to the presence of the LCBs. Fig. 5b shows that wave skewness stays around zero at a small Ursell number, then increases slowly up to a maximum value from zero, and finally starts to decrease slowly. It is interesting to observe that wave skewness is larger than that on the incident side under the same Ursell number (Figs. 5a and b). Elgar and Guza (1985), Crawford (2000) and Crawford and Hay (2001) have suggested that wave energy at high frequencies enhances sum frequency interactions, therefore generating more positive skewness, and this could be an explanation for our observation. As shown in Fig. 5d, wave asymmetry increases rapidly up to maximum value from zero then decays slowly with increasing Ursell number. Wave asymmetry on the transmission side also has a maximum value comparing with that on the incident side. The empirical Eqs. (4) and (5) are derived from the measurements on the transmission side using least squares fitting to relate S_t and A_t to U_{rt}. Predictions agree well with observations for wave skewness ($R^2 = 0.70$) and reasonably well for wave asymmetry ($R^2 = 0.62$). It should be stated that the range of Ursell number on the transmission side is between 0.05 and 12.5.

$$S_t = -1.25^{*}\tanh\left(\frac{3.19}{U_{rt}}\right) + 1.23 \tag{4}$$

$$A_t = -0.015^{*}U_{rt}^2 + 0.19^{*}U_{rt} - 0.05. \tag{5}$$

3.2. Transformation of wave skewness and asymmetry over rubble mound LCBs

The water depths used in the rubble mound LCBs are 0.05 m smaller than those of smooth LCBs, the nominal diameter of the units in the rubble mound LCBs is $D_{n50} = 0.047$ m, and the seaside slope is 1:2 for rubble mound LCBs, whereas it is 1:3 for smooth LCBs.

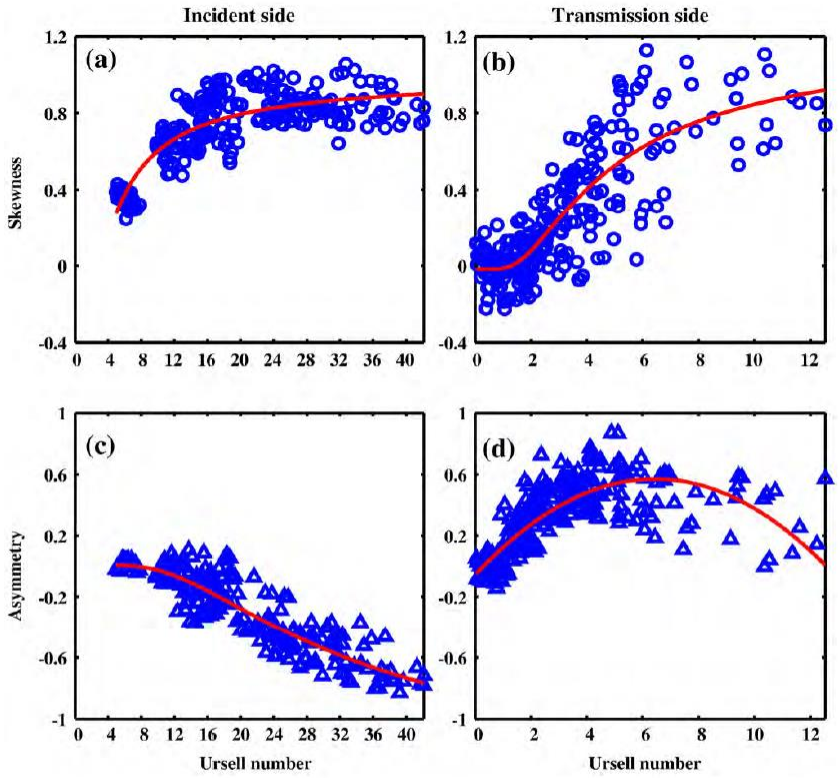

Fig. 5. Relationship between wave skewness (a and b) and asymmetry (c and d) and Ursell number on the incident side (left panel) and the transmission side (right panel) of smooth LCBs. Solid line is predicted by Eq. (2) for (a), Eq. (3) for (c), Eq. (4) for (b) and Eq. (5) for (d).

Figs. 6a and c show that the relationships of rubble mound LCBs between wave asymmetries and the Ursell number are similar to those of smooth LCBs on the incident side. This may be due to the reflection from the incident side of both LCBs which is minimized in order to focus on wave transmission in the design of the DELOS project (Van der Meer et al., 2005; Kramer et al., 2005). Eqs. (6) and (7), derived by least squares fitting, specify these relationships with $R^2 = 0.64$ and $R^2 = 0.84$ for wave skewness and asymmetry respectively. The range of Ursell number on the incident side is between 6 and 66. Comparisons between Eqs. (6) and (7) of rubble mound LCBs and Eqs. (2) and (3) of smooth LCBs are shown in Fig. 6. There is not much difference in the comparisons of empirical formulae between rubble mound LCBs and smooth LCBs, although there is some underestimation of wave skewness by Eq. (2) of smooth LCBs.

$$S_i = -11.32^* \tanh\left(\frac{0.42}{U_{ri}}\right) + 1.17 \tag{6}$$

$$A_i = -1.23^* \tanh\left(\frac{-15.82}{U_{ri}}\right) - 1.16. \tag{7}$$

We will next examine the relationships between wave skewness and asymmetry and the Ursell number on the transmission side of rubble mound LCBs. Fig. 6b shows that wave skewness stays around zero at a small Ursell number, then increases slowly up to a maximum value from zero, and finally begins to decay. Wave asymmetry increases quadratically with increasing Ursell number from approximately zero, reaches the maximum of wave skewness, then decays quadratically low to negative values (Fig. 6d). The recommended formulae for rubble mound LCBs are:

$$S_t = 2.97^* \tanh\left(\frac{-9.16}{U_{rt}}\right) + 3.04 \tag{8}$$

$$A_t = -0.015^* U_{rt}^2 + 0.22^* U_{rt} - 0.41 \tag{9}$$

where R^2 is 0.72 for Eq. (8) and 0.54 for Eq. (9). The applicable range of Ursell number on the transmission side is 1.5 to 15.

Fig. 6 shows comparisons between Eqs. (8) and (9) of rubble mound LCBs and Eqs. (4) and (5) of smooth LCBs. Predictions of wave asymmetries for rubble mound LCBs are smaller than those of smooth LCBs, although they are both around zero values at small Ursell numbers. This may be due to the roughness and porosity of the structure, causing energy dissipation, which consequently decreases wave nonlinear interactions and generates small wave asymmetries.

Since wave skewness and asymmetry are related to net sediment transport, the investigations above provide effective ways to predict wave asymmetries, which may help incorporate wave asymmetries into analytic or numerical models of the sediment transport, consequently may help improve the breakwaters stable and decrease sediment transport.

4. Relationships of wave asymmetries between both sides of SLCBs

Although wave skewness and asymmetry are strongly related to a local Ursell number as discussed above, it is worthwhile investigating

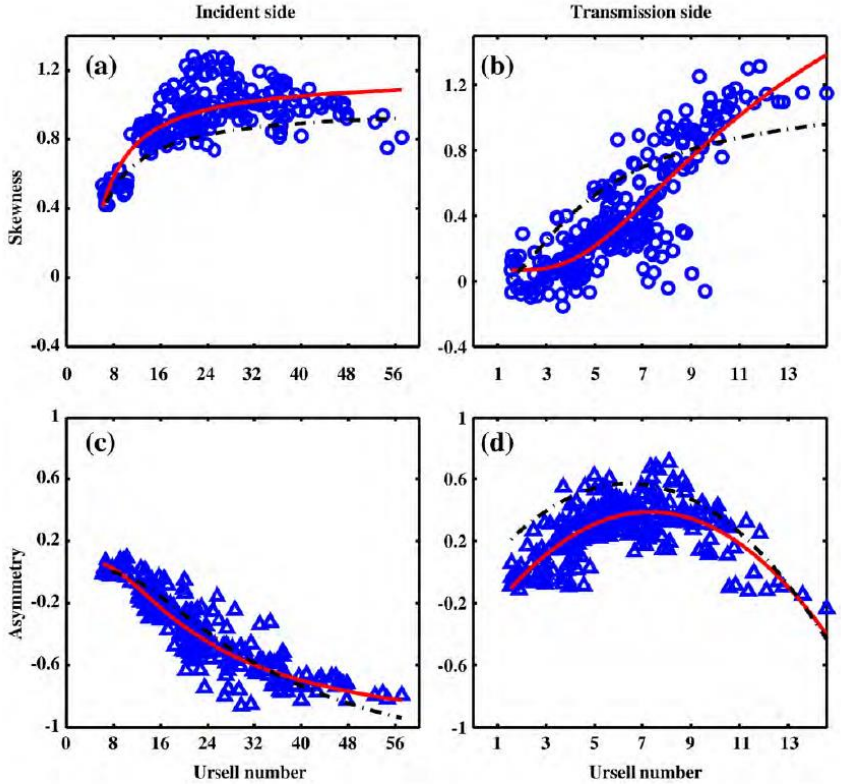

Fig. 6. Relationship between wave skewness (a and b) and asymmetry (c and d) and Ursell number on the incident side (left panel) and the transmission side (right panel) of rubble mound LCBs. Solid line is predicted by Eq. (6) for (a), Eq. (7) for (c), Eq. (8) for (b) and Eq. (9) for (d). The dash-dotted lines are predicted using Eq. (2) for (a), Eq. (3) for (c), Eq. (4) for (b) and Eq. (5) for (d) respectively.

the relationships of wave asymmetries between both sides of LCBs. This helps to understand the effect of the presence of LCBs on wave transformation over LCBs. Fig. 7 shows that for smooth LCBs, wave skewness on the transmission (S_t) side stays around zero, and then has weakly linear independence on wave skewness on the incident side (S_i), while wave asymmetry on the transmission side (A_t) has weakly quadratic independence on wave asymmetry on the incident side (A_i). The effect of the relative freeboard on the relationships of wave asymmetries between both sides of LCBs is not significant. Wave skewness retains a positive sign on both sides but asymmetry changes from negative on the incident side to positive on the transmission side. For rubble mound LCBs, wave skewness on the transmission side shows linear dependence on wave skewness on the incident side, and wave asymmetry on the transmission side displays a weakly quadratic dependence on wave asymmetry on the incident side. The effect of the relative freeboard on the relationships of wave asymmetries on both sides of LCBs is significant: under the same S_i or A_i, large relative freeboards correspond to small S_t or A_t respectively. This is due to a considerable increase in the intensity of wave breaking as the relative freeboard increased (Blenkinsopp and Chaplin, 2008), consequently more energy is dissipated, which decreases wave nonlinear interactions and generates small wave asymmetries. For wave transformation of both smooth and rubble mound LCBs, wave asymmetry changes the sign from negative to positive, corresponding to waves pitching forward to pitching backward (Fig. 2). This is consistent with previous research results over a submerged sand bar on a beach (Herbers et al., 2003). Note that Herbers et al.'s definition of wave asymmetry has the opposite sign to that in the present work and also to that of Elgar and Guza's (1985).

5. Bispectral analysis of nonlinear wave interactions

With the presence of LCBs, waves retain a sharp crest and flat trough on both sides but change from pitch forward to pitch backward, which in turn may change the directions in wave induced sediment transport, consequently modifying the beach morphology after construction of the LCBs. To better understand the transformation of wave asymmetries analyzed above, bispectral analysis has been applied here to study the contributions to the wave skewness and asymmetry from the interactions of different wave frequencies, as done by Elgar and Guza (1985).

In waves that are initially linear, nonzero wave skewness and asymmetry arises as a result of nonlinear interaction between the frequency constituents of the waves during the shoaling process. Bispectral analysis has been introduced to investigate the contribution of nonlinear interactions between frequency components of wave spectrum by previous researchers (Elgar and Guza, 1985; Doering and Bowen, 1995), since the bispectrum is usually used to detect the secondary forced waves and can apparently show the phase coupling between the primary waves and associated forced waves.

The digital complex bispectral estimate $B(f_1, f_2)$ for discretely sampled data can be interpreted in terms of Fourier coefficients, (Haubrich, 1965; Kim and Powers, 1978), as

$$B(f_1, f_2) = E[A(f_1)A(f_2)A^*(f_3)] \tag{10}$$

where $E[\ ]$ denotes an expected value, $A(f)$ denotes a complex Fourier coefficient, while the asterisk represents a complex conjugate.

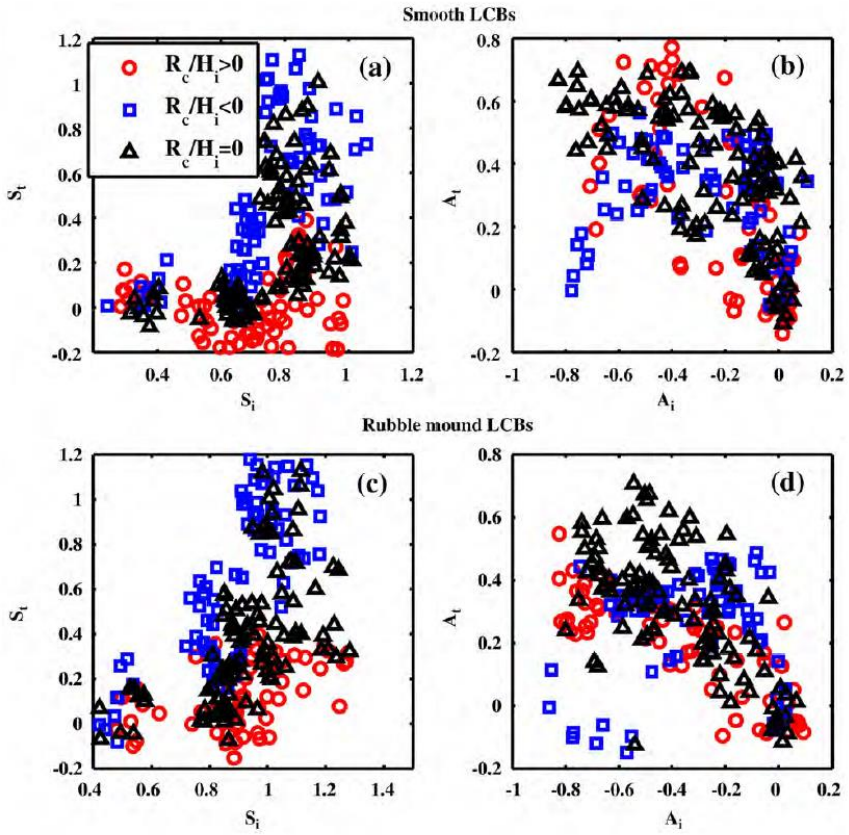

Fig. 7. Relationships of wave asymmetries between both sides of LCBs. (a) Wave skewness of smooth LCBs, (b) wave asymmetry of smooth LCBs, (c) wave skewness of rubble mound LCBs and (d) wave asymmetry of rubble mound LCBs.

f_i (i = 1, 2, 3) are wave frequencies and conventionally $f_3 = f_1 + f_2$. For example, if $B(0.59, 0.59) = 0.5$, this indicates a self–self interaction at frequency $f = 0.59$ coupling to energy at frequency $f = 1.18$ Hz.

In the work of Kim and Powers (1978), the normalized magnitude of the bispectrum was used to define the bicoherence, b.

$$b^2(f_1, f_2) = \frac{|B(f_1, f_2)|^2}{E[|A_{f_1} A_{f_2}|^2] E[|A_{f_1+f_2}|^2]}. \tag{11}$$

Elgar and Guza (1985) concluded that the bicoherence does represent the relative degree of phase coupling between triads of waves. For example, with $b = 1$ for full coupling, and $b = 0$ for random phase relationships. Significant peaks in bicoherence identify two frequencies of the three in an interacting triad contributing significant energy to the time series.

Hasselman et al. (1963) and Elgar and Guza (1985) indicated that the mean cube or third moments of a stationary random time series, denoted here by $\eta(t)$, can be related to the integral of the parts of the bispectrum if f_1 is greater than f_2. For example, wave skewness, S, can be expressed as

$$S = \frac{\sum\sum \Re\{B(f_1, f_2)\}}{E(\eta(t)^2)^{3/2}} \tag{12}$$

Similarly, wave asymmetry, A, was defined as the integral of the imaginary part of the bispectrum (Elgar and Guza, 1985)

$$A = \frac{\sum\sum \Im\{B(f_1, f_2)\}}{E(\eta(t)^2)^{3/2}} \tag{13}$$

where $\Im\{\}$ and $\Re\{\}$ denote the imaginary and real parts of the bispectrum respectively.

In the Delos datasets, the generated spectrum initially has only one peak at the primary frequency and keeps the same for cases with negative and zero freeboards, but it evolves to double peaks around the primary frequency for the cases with the positive freeboard due to significant wave reflections. For the case of the LCB with the negative freeboard (Fig. 8), the spectrum on the incident side has a large peak at the primary frequency $f = 0.5$ Hz and a small peak at the second harmonic frequency $f = 1.0$ Hz, while the spectrum on the transmission side is a broader power spectrum, although the primary frequency is also 0.5 Hz. This is consistent with the investigation by Van der Meer et al. (2005). However, for the case of the LCB with the positive freeboard (Fig. 9), the spectrum on the incident side shows three peaks, which locate at $f = 0.48$ Hz, $f = 0.6$ Hz, and a higher frequency peak at $f = 1.2$ Hz respectively. Transmitted waves are characterised by a broader power spectrum, peak frequencies are $f = 0.58$ Hz and $f = 1.1$ Hz respectively. In the present work, bispectral analysis is implemented next for the cases of smooth LCB with the negative freeboard (Fig. 8) and positive freeboard (Fig. 9). There are 281 degrees of freedom and the 95% significant level for zero bicoherence is $b = 0.146$ (Haubrich, 1965), and significant nonzero values in the bispectrum are limited to frequencies below 2 Hz. Areas of significant bicoherence indicate frequency pairs (f_1, f_2) that are involved in either sum or difference interactions. The bispectrum was normalized by $E(\eta(t)^2)^{\frac{3}{2}}$. The sign of $\Re\{B\}$ and $\Im\{B\}$ at frequencies (f_1, f_2) describe the sign of the contribution to the overall skewness and asymmetry arising from the nonlinear interactions. The relationships between wave skewness and asymmetry and the bispectrum are defined by Eqs. (12) and (13).

In Fig. 8c, the bicoherence on the incident side indicates strong coupling at the peaks ($f_1 = 0.5$ Hz, $f_2 = 0.5$ Hz) and ($f_1 = 1.0$ Hz, $f_2 = 0.5$ Hz) with $b = 0.35$, while on the transmission side (Fig. 8d), the bicoherence indicates strong coupling at the peak ($f_1 = 0.5$ Hz, $f_2 = 0.5$ Hz) with $b = 0.35$ and frequency pairs ($f_1 = 0.7$ Hz, $f_2 = 0.5$ Hz) and ($f_1 = 0.9$ Hz, $f_2 = 0.5$ Hz) with $b = 0.25$. It is obvious that wave nonlinear coupling on the peaks and harmonics on the incident side is greater than that on the transmission side. As shown in Figs. 8e and f, on the incident side, $\Re\{B(f_1, f_2)\}$ has a large positive value around the frequency pairs ($f_1 = 0.5$ Hz, $f_2 = 0.5$ Hz) and also has a small positive value at the frequency pairs ($f_1 = 1.0$ Hz, $f_2 = 0.5$ Hz); while on the transmission side, $\Re\{B(f_1, f_2)\}$ is positive under the self–self interaction ($f_1 = 0.5$ Hz, $f_2 = 0.5$ Hz) with large bicoherence. Positive $\Re\{B(f_1, f_2)\}$of self–self interaction and sum interactions between peak frequency and second harmonic, leads to an overall positive skewness, which is concurrently also consistent with that in Fig. 2. Fig. 8g demonstrates that on the incident side, $\Im\{B(f_1, f_2)\}$ is negative around the frequency pairs ($f_1 = 0.5$ Hz, $f_2 = 0.5$ Hz) with large bicoherence. The large negative $\Im\{B(f_1, f_2)\}$ induced by self–self interaction leads to an overall negative asymmetry although there are small positive values. However, Fig. 8h shows that $\Im\{B(f_1, f_2)\}$ the transmission side has large positive values around the frequency pairs ($f_1 = 0.5$ Hz, $f_2 = 0.7$ Hz) and ($f_1 = 0.5$ Hz, $f_2 = 0.9$ Hz). The couplings between $f_1 = 0.5$ Hz and $f_2 = 0.7$ Hz and $f_1 = 0.5$ Hz and $f_2 = 0.9$ Hz correspond to the difference interactions between $f_1 = 0.5$ Hz and $f_3 = 1.2$ Hz and $f_1 = 0.5$ Hz and $f_3 = 1.4$ Hz, transferring energy into the spectral valley between 0.5 Hz and 1.4 Hz. The large positive $\Im\{B(f_1, f_2)\}$ induced by difference interactions leads to an overall positive asymmetry.

Comparing with the case of the negative freeboard, the case with the positive freeboard is analyzed and shown in Fig. 9. The bicoherence indicates strong coupling around the peaks ($f_1 = 0.6$ Hz, $f_2 = 0.48$ Hz) and ($f_1 = 1.2$ Hz, $f_2 = 0.48$ Hz) with $b = 0.45$ on the incident side and the frequency pairs ($f_1 = 0.58$ Hz, $f_2 = 0.52$ Hz) with $b = 0.45$ on the transmission side. Fig. 9e and f shows that on the incident side, $\Re\{B(f_1, f_2)\}$ is positive around frequency pairs ($f_1 = 0.6$ Hz, $f_2 = 0.48$ Hz) and ($f_1 = 1.2$ Hz, $f_2 = 0.48$ Hz), and on the transmission side $\Re\{B(f_1, f_2)\}$ is positive at the frequency pairs ($f_1 = 0.58$ Hz, $f_2 = 0.58$ Hz) with self–self interaction. Therefore, the large positive $\Re\{B(f_1, f_2)\}$, induced by self–self interaction and interactions between peak frequency and higher frequency, leads to an overall positive skewness. As seen in Fig. 9g, on the incident side, the peak ($f_1 = 0.6$ Hz, $f_2 = 0.48$ Hz) has negative $\Im\{B(f_1, f_2)\}$ showing a sum interaction between frequencies $f_1 = 0.6$ Hz and $f_2 = 0.48$ Hz, as well as the sum interaction between frequency pairs ($f_1 = 1.2$ Hz, $f_2 = 0.48$ Hz). Both sum interactions have large bicoherence. The large negative $\Im\{B(f_1, f_2)\}$ induced by sum interactions between frequency pairs, leads to an overall positive asymmetry. On the transmission side, Fig. 9h describes positive $\Im\{B(f_1, f_2)\}$ of large magnitude arising from the coupling between $f_1 = 0.58$ Hz and $f_2 = 0.52$ Hz with $b = 0.45$, corresponding to a difference interaction between $f_1 = 0.58$ Hz and $f_3 = 1.1$ Hz transferring energy into the spectral valley around the frequency of 0.52 Hz. Large positive $\Im\{B(f_1, f_2)\}$ induced by difference interactions with large bicoherence leads to an overall positive asymmetry.

6. Conclusions and discussions

The present work describes the transformation of wave skewness and asymmetry when waves propagate over a smooth and a rubble mound LCB. The analysis was based on measurements collected in the DELOS project. On the incident side of smooth LCBs, wave skewness is positive and increases with the increasing Ursell number then stays around the maximum, and wave asymmetry is negative and decays with the increasing Ursell number. On the transmission side of smooth LCBs, wave skewness shows similar dependence on the Ursell number to that on the incident side, but wave skewness is larger than that on the incident side under the same Ursell number, while wave asymmetry is positive and increases rapidly up to a maximum then decays slowly with increasing U_r. Several practical empirical formulae relating wave skewness and asymmetry to Ursell number are established using least squares fitting for practical use. Predictions are in good agreement with measurements.

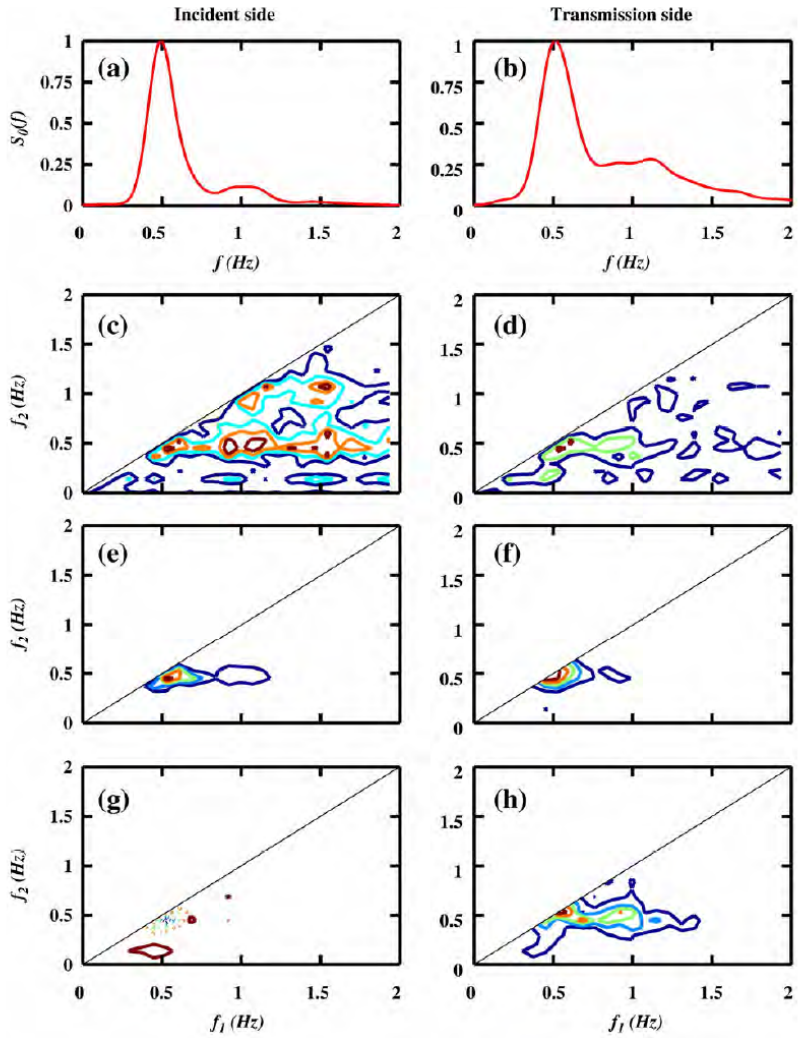

Fig. 8. Normalized power spectra (a and b), contours of bicoherence (c and d), contours of real part (e and f) and imaginary part (g and h) of normalized bispectrum on the incident side (left column) and transmission side (right column) of smooth LCBs ($R_c = -0.05$ m, $H_i = 0.13$ m, $h = 0.35$ m, $\alpha = 0°$). The minimum levels of contour plots are (c) 0.15, (d) 0.15, (e) 2e–4, (f) 2e–4, (g) −11e–4 and (h) 0.6e–4. The corresponding intervals of contour levels are 0.1, 0.1, 3e–4, 3e–4, 3e–4, and 1.5e–4 respectively. Dashed contours are negative values and solid ones are positive values.

Although relationships between wave asymmetries and the Ursell number of rubble mound LCBs are similar to those of smooth LCBs, wave skewness and asymmetry on the transmission side of the rubble mound are smaller than those of smooth LCBs under the same Ursell number, although they are both around zero at small Ursell numbers.

Wave skewness on the transmission side of smooth LCBs show linear dependence on wave skewness on the incident side, while wave asymmetry on the transmission side display weakly quadratic dependence on wave asymmetry on the incident side. Although wave asymmetries on the transmission side of rubble mound LCBs display similar dependence on wave asymmetries on the incident side as that of smooth LCBs, the effect of the relative freeboard on the relationships of wave asymmetries between both sides is significant for rubble mound LCBs, but not significant for smooth LCBs. Wave skewness retains a positive sign on both sides but asymmetry changes from negative on the incident side to positive on the transmission side.

Our bispectral analysis shows that positive skewness and negative asymmetry arises from self–self and sum interactions between frequency components of waves; the main contribution to positive asymmetry is due to difference interactions between the two principal components of waves on the transmission side of LCBs.

As is widely known, water waves shoal and adapt to the local depth in front of structures, then break and transmit in the vicinity of structures. The wave transmission effect is greatest directly behind the structures, but after several wave periods, waves recover to be Rayleigh distributed in uniform water depth. However, experimental datasets are limited to the vicinity of the structures, and in the future it would be helpful for us to look at the development of waves behind

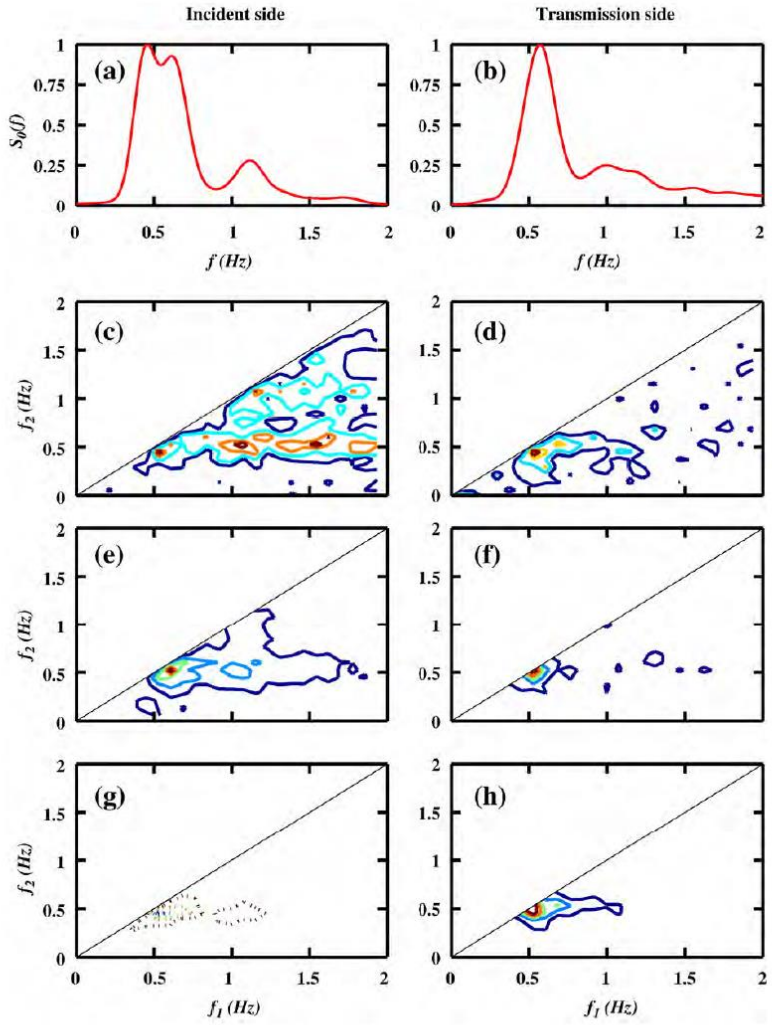

Fig. 9. Normalized power spectra (a and b), contours of bicoherence (c and d), contours of real part (e and f) and imaginary part (g and h) of normalized bispectrum on the incident side (left column) and transmission side (right column) of smooth LCBs ($R_c = 0.05$ m, $H_i = 0.11$ m, $h = 0.25$ m, $\alpha = 0°$). The minimum levels of contour plots are (c) 0.15, (d) 0.15, (e) 1e–4, (f) 1e–4, (g) −13e–4 and (h) 2e–4. The corresponding intervals of contour levels are 0.1, 0.1, 2e–4, 3e–4, 3e–4, and 3e–4 respectively. Dashed contours are negative values and solid ones are positive values.

the structure towards the land to give guidance about the application in a wider area behind the structure.

7. List of symbols

η_i	Wave surface elevation (m)
S	Wave skewness. $S = \frac{\langle(\eta_i - \bar{\eta}_i)^3\rangle}{\langle(\eta_i - \bar{\eta}_i)^2\rangle^{\frac{3}{2}}}$ (−)
A	Wave asymmetry. The skewness of the Hilbert transform of surface elevation (−)
S_i	Wave skewness on the incident side of breakwaters (−)
S_t	Wave skewness on the transmission side of breakwaters (−)
A_i	Wave asymmetry on the incident side of breakwaters (−)
A_t	Wave asymmetry on the transmission side of breakwaters (−)
h	Local water depth (m)
H_s	Local significant wave height (m)
H_i	Incident significant wave height, preferably H_s at the location of gauge 1. (m)
T_{m01}	Wave mean period, $T_{m01} = 2{*}\pi{*}m_0/m_1$ (s)
L_m	Local mean wave length calculated with T_{m01} (m)
U_r	Ursell number, $U_r = \frac{H_i L_m^2}{h^3}$ (−)
U_{ri}	Ursell number on the incident side of breakwaters (−)
U_{rt}	Ursell number on the transmission side of breakwaters (−)
$\frac{R_c}{H_i}$	Relative freeboard (−)
B	Seaside slope of LCBs (°)
T_{p0}	Peak period of incident waves collected at the location of gauge 1 (s)
L_0	Wave length in deep water (m)
sop	Wave steepness $S_{op} = \frac{2\pi H_i}{gT_{p0}^2} = \frac{H_i}{L_0}$ (−)
ξ	Iribarren number $\xi = \tan(\beta)/(sop)^{0.5}$ (−)
α	Incident wave angle (°)

s	Spreading parameter (−)
D_{n50}	Nominal diameter of rubbles (m)
B	Crest width of LCBs (m)

Acknowledgements

This work was based on the data sets of the EU-funded project DELOS "Environmental Design of Low Crested Coastal Defence Structures" (EVK3-2000-00041). The authors acknowledge the support of the Natural Environmental Research Council (Grant No. NE/E002129/1) and the Engineering and Physical Sciences Research Council (Grant no. EP/C013085/1), along with Dr Anna M. Crawford who generously supplied her bispectrum code. This work was carried out while Zhong Peng was in receipt of a University of Plymouth postgraduate research scholarship.

References

Bagnold, R.A., 1966. An approach to the sediment transport problem from general physics. US Geological Survey Professional Paper 422-I, 37.

Bailard, J.A., Inman, D.L., 1981. An energetics bedload model for a plane sloping beach: local transport. Journal of Geophysical Research 86 (C3), 2035–2043.

Blenkinsopp, C.E., Chaplin, J.R., 2008. The effect of relative crest submergence on wave breaking over submerged slopes. Coastal Engineering 55 (12), 967–974.

Bowen, A.J., 1980. Simple models of nearshore sedimentation; beach profiles and longshore bars. In: McCann, S.B. (Ed.), The Coastline of Canada. Geological Survey of Canada, pp. 1–11.

Christou, M., Swan, C., Gudmestad, O.T., 2008. The interaction of surface water waves with submerged breakwaters. Coastal Engineering 55 (12), 945–958.

Cornish, V., 1898. On sea beaches and sandbanks. Geographical Journal 11 (5), 528–543.

Crawford, A.M., 2000. Field observations of linear transition ripple migration and wave orbital velocity skewness. PhD thesis Thesis, Memorial Univeristy of Newfoundland, Newfoundland.

Crawford, A.M., Hay, A.E., 2001. Linear transition ripple migration and wave orbital velocity skewness: observations. Journal of Geophysical Research-Oceans 106 (C7), 14113–14128.

Doering, J.C., Bowen, A.J., 1995. Parametrization of orbital velocity asymmetries of shoaling and breaking waves using bispectral analysis. Coastal Engineering 26, 15–33.

Doering, J.C., Elfrink, B., Hanes, D.M., Ruessink, G., 2000. Parameterization of velocity skewness under waves and its effect on cross-shore sediment transport. In: Edge, B.L. (Ed.), Proceedings of the 27th International Conference of Coastal Engineering. Sydney, Australia, pp. 1383–1397.

Drake, T.G., Calantoni, J., 2001. Discrete particle model for sheet flow sediment transport in the nearshore. Journal of Geophysical Research 106 (C9), 19859–19868.

Elgar, S., Guza, R.T., 1985. Observations of bispectra of shoaling surface gravity waves. Journal of Fluid Mechanics 161, 425–448.

Hasselman, K., Munk, W., MacDonald, G., 1963. Bispectra of ocean waves. In: Rosenblatt, M. (Ed.), Time Series Analysis. Wiley, pp. 125–139.

Haubrich, R.A., 1965. Earth noise, 5 to 500 millicycles per second. 1. Spectral stationarity, normality and nonlinearity. Journal of Geophysical Research 70 (6), 1415–1427.

Herbers, T.H.C., Orzech, M., Elgar, S., Guza, R.T., 2003. Shoaling transformation of wave frequency-directional spectra. Journal of Geophysical Research-Oceans 108 (C1).

Inman, D.L., Bagnold, R.A., 1963. Littoral processes. In: Hill, M.N. (Ed.), The sea. Interscience, New York, pp. 529–533.

Kim, Y.C., Powers, E.J., 1978. Digital bispectral analysis of self-excited fluctuation spectra. Physics of Fluids 21 (8), 1452–1453.

Kramer, M., Zanuttigh, B., van der Meer, J.W., Vidal, C., Gironella, F.X., 2005. Laboratory experiments on low-crested breakwaters. Coastal Engineering 52 (10–11), 867–885.

Nielsen, P., 1992. Coastal Bottom Boundary Layers and Sediment Transport. In: Advanced Series on Ocean Engineering, vol. 4. World Scientific, Singapore. 324 pp.

Nielsen, P., Callaghan, D.P., 2003. Shear stress and sediment transport calculations for sheet flow under waves. Coastal Engineering 47 (3), 347–354.

Phillips, O.M., 1960. On the dynamics of unsteady gravity waves of finite amplitude. Journal of Fluid Mechanics 9, 193–217.

Stokes, G.G., 1847. On the theory of oscillatory waves. Transactions of the Cambridge Philosophical Society 8, 441–455.

Van der Meer, J.W., Regeling, E., de Waal, J.P., 2000. Wave transmission: spectral changes and its effects on run-up and overtopping. In: Edge, B.L. (Ed.), Proceedings of the 27th International Conference of Coastal Engineering. Sydney, Australia, pp. 2156–2168.

Van der Meer, J.W., Briganti, R., Zanuttigh, B., Wang, B.X., 2005. Wave transmission and reflection at low-crested structures: Design formulae, oblique wave attack and spectral change. Coastal Engineering 52 (10–11), 915–929.

Wang, B., 2003. Oblique wave transmission at low-crested structures. MSc. Thesis Thesis, Institute for Water Education.

Wang, B.X., Otta, A.K., Chadwick, A.J., 2007. Transmission of obliquely incident waves at low-crested breakwaters: theoretical interpretations of experimental observations. Coastal Engineering 54 (4), 333–344.

Wilson, K.C., 1966. Bed-load transport at high shear stress. Journal of the Hydraulic Division 92, 49–59.

Zou, Q.P., Hay, A.E., Bowen, A.J., 2003. The vertical structure of surface gravity waves propagating over a sloping sea bed: theory and field measurements. Journal of Geophysical Research 108 (C8), 3265. doi:10.1029/2002JC001432.